Sun Wei-Jie (Orcid ID: 0000-0001-5260-658X)
Raines Jim, M (Orcid ID: 0000-0001-5956-9523)
Fu Suiyan (Orcid ID: 0000-0002-3858-1555)
Slavin James, A. (Orcid ID: 0000-0002-9206-724X)
Wei Yong (Orcid ID: 0000-0001-7183-0229)
Poh Gangkai (Orcid ID: 0000-0002-5775-2006)
Pu Zuyin (Orcid ID: 0000-0002-8458-6648)
Zong Qiu-Gang (Orcid ID: 0000-0002-6414-3794)

MESSENGER observations of the energization and heating of protons in the near Mercury magnetotail

W. J. Sun [1,2,3], J. M. Raines [4], S. Y. Fu [3], J. A. Slavin [4], Y. Wei [1], G. K. Poh [4], Z. Y. Pu[3], Z. H. Yao [5], Q. G. Zong[3], W. X. Wan [1]

Corresponding author: W. J. Sun (weijiesun@pku.edu.cn)

[1] Key Laboratory of Earth and Planetary Physics, Institute of Geology and Geophysics, Chinese Academy of Sciences, Beijing 100029, China.

[2] Key Laboratory of Lunar and Deep Space Exploration, National Astronomical Observatories, Chinese Academy of Sciences, Beijing 100012, China.

[3] School of Earth and Space Sciences, Peking University, Beijing 100871, China.

[4] Department of Climate and Space Sciences and Engineering, University of Michigan, Ann Arbor, Michigan, USA.

[5] Laboratoire de Physique Atmosphérique et Planétaire, STAR Institute, Université de Liège, Liège, Belgium.

This is the author manuscript accepted for publication and has undergone full peer review but has not been through the copyediting, typesetting, pagination and proofreading process, which may lead to differences between this version and the Version of Record. Please cite this article as doi: 10.1002/2017GL074276

Abstract.

The energization and heating processes for protons in the near Mercury tail are examined with MESSENGER observations. In a case study, supra-thermal proton particle flux (STPF) and proton temperature are observed to be clearly enhanced during near-Mercury substorm dipolarizations, indicating the proton energization and heating processes. STPF and proton temperature distributions in near-Mercury central plasma sheets display dawn-dusk asymmetries, with higher values in the dawnside plasma sheet, i.e., post-midnight, than in the duskside, i.e., pre-midnight. Further investigations reveal that these asymmetries are more prominent during active periods in Mercury's magnetosphere, as compared to quiet periods. Magnetic field variations in the Z_{MSM} component display a similar feature, with variations being more prominent on the dawnside than the duskside during active periods. We propose that the dawn-dusk asymmetry in the distributions of protons could be due to the fact that more substorm dipolarizations were initiated on the dawnside of Mercury's magnetotail.

1. Introduction

Observations from the MErcury Surface, Space ENvironment, GEochemistry, and Ranging (MESSENGER) have revealed that Mercury's magnetosphere is similar to the Earth in many aspects, while also exhibiting some differences. For example, the magnetotail substorm activities of plasma sheet thinning and increasing magnetic field intensity during the growth phase followed by plasma sheet thickening and field intensity decreasing during the expansion phase are similar to what is observed at Earth. However, at Mercury they are observed with much shorter time scales, of 2 – 3 minutes, rather than the 2 – 3 hours observed at Earth [*Slavin et al.*, 2010; *Sun et al.*, 2015a, 2015b].

To study the ion properties in Mercury's magnetotail, *Gershman et al.* [2014] have investigated several tens of pre-midnight plasma sheet crossings at distances down the tail of ~ 2 - 3 R_M (R_M, Mercury radius ~ 2440 km) in the Near Mercury Neutral Line (NMNL) region [e.g., *Slavin et al.*, 2012; *DiBraccio et al.*, 2015; *Poh et al.*, 2017a]. In that study, ion species (such as, H^+, He^{++}, and Na^+) in Mercury's plasma sheet display strong kinetic effects. In another statistical study on the mean proton flux, the flux was found to be higher near the dawnside magnetopause. Also a pronounced north-south asymmetry was found due to the northward offset (~ 0.2 R_M) of Mercury's dipole [*Korth et al.*, 2014].

Substorm dipolarization observed by MESSENGER at 2011 and 2012 lasted only ~ 5 s during Mercury's magnetospheric substorms [*Sun et al.*, 2015a, 2015b]. Energetic electron events possibly associated with dipolarizations at Mercury were first reported with Mariner 10 observations in the 1970s [e.g., *Christon et al.*, 1979; *Christon*, 1987; *Slavin et al.*, 1997]. MESSENGER measurements have provided more comprehensive

investigations of the energetic electron distributions, which have displayed clear dawn-dusk asymmetries with more energetic electron events detected in the dawnside of the magnetosphere [e.g., *Baker et al.*, 2016; *Ho et al.*, 2016; *Lindsay et al.*, 2016]. Further, *Lindsay et al.* [2016] found that the MESSENGER X-ray Spectrometer (XRS) observed a dawnside maximum in X-ray emissions from Mercury's surface. They interpreted these emissions in the XRS data as being due to the precipitation of energetic electrons preferentially from the dawnside plasma sheet. This dawn-dusk asymmetry feature for energetic electrons was explained in terms of the dawnward drift of electrons. In a later study, *Sun et al.* [2016] found that magnetic reconnection occurs more frequently in the dawnside plasma sheet of NMNL region. They proposed that energetic electrons could be locally generated in the dawnside near Mercury tail, thus contributing to the dawn-dusk asymmetry.

Since the timescale of dipolarization is comparable with the gyro-period of proton in the Mercury's plasma sheet [*Sundberg et al.*, 2012; *Sun et al.*, 2015a; *Sundberg and Slavin*, 2015], it would be very interesting to check the influences of dipolarization on the protons at Mercury. Test-particle simulations show that protons can be energized up to a few tens keV during the dipolarizations (5 s and 10 s) at Mercury [e.g., *Ip*, 1997; *Delcourt et al.*, 2007]. In the work of *Sun et al.* [2015a], they have shown the possible energization of protons during Mercury's substorm dipolarization with MESSENGER observations. However, a detailed analysis for proton behaviors during Mercury's substorm dipolarizations is still lacking.

In studies at Earth, dawn-dusk asymmetry features with higher occurrence rates in the duskside tail have been extensively investigated, including magnetic reconnection at the Near Earth Neutral Line (NENL) region [e.g., *Nagai et al.*, 1998, 2013] as well as

ion and electron dispersionless injections in the near-Earth plasma sheet [e.g., *Lopez et al.*, 1990; *Gabrielse et al.*, 2014]. At Mercury, higher occurrence rates of magnetic reconnection in the dawnside NMNL have been observed [*Sun et al.*, 2016], that contrast with observations at Earth. These results provide further motivation for the investigation of proton properties in the near Mercury tail.

In this work, we investigate the proton properties in the near Mercury tail with MESSENGER observations. We study the energization and heating processes for protons during Mercury's substorm dipolarization. We use supra-thermal proton particle flux and proton temperature (T_p) distributions as well as the magnetic field Z (B_z) component variations. We compare the distributions of supra-thermal protons in the near Mercury tail with those observed at Earth.

2. Observations

In this study, we utilize magnetic field data (20 samples per second) from magnetometer (MAG) [*Anderson et al.*, 2007] onboard MESSENGER [*Solomon et al.*, 2007]. The MAG data is provided in Mercury solar magnetospheric coordinates (MSM), in which X_{MSM} and Z_{MSM} axes are sunward and parallel to the dipole axis, respectively, and Y_{MSM} axis completes the right-handed system. Spacecraft position data are provided with the same resolution as MAG data. We have adopted an aberrated coordinate system by clockwise rotating (viewing from the positive Z_{MSM}) the X_{MSM}-Y_{MSM} plane so that X'_{MSM} is anti-parallel to the solar wind velocity vector (~ 400 km/s), which itself is aberrated from the radial direction by Mercury's orbital motion around the Sun. The spacecraft locations in the tail in aberrated MSM coordinate system would have a dawnward offset comparing to MSM coordinate

system. The dawnward offset is smaller the closer to the planet. And the aberrated coordinate system is very necessary in the study of dawn-dusk features for Mercury tail dynamics.

Proton measurements used in this study are provided by the Fast Imaging Plasma Spectrometer (FIPS) with an energy range from ~ 46 eV/e to ~ 13.7 keV/e in a scan time of ~ 10 s [*Andrews et al.*, 2007]. FIPS images an effective field of view of ~ 1.15π sr. Proton moments (number density, n_p, and temperature, T_p) were derived through 1 minute averaging of E/q distributions under the assumption of isotropic and stationary Maxwellian distributions [*Raines et al.*, 2011; *Gershman et al.*, 2013]. This semi-analytical method of computing proton moments has been applied successfully in many regions at Mercury, such as the plasma depletion layer in the magnetosheath [*Gershman et al.*, 2013; *Slavin et al.*, 2014], the cusp [*Zurbuchen et al.*, 2011; *Raines et al.*, 2014; *Slavin et al.*, 2014], and the plasma sheet [*Raines et al.*, 2011; *Gershman et al.*, 2014; *Poh et al.*, 2017a].

2.1. Case Studies

Proton and magnetic field observations from two passes of MESSENGER through Mercury's plasma sheet on July 1, 2011 and September 28, 2011 are presented in Figure 1. Clear magnetospheric substorm growth and expansion phase signatures have already been identified in the July 1st event [*Sun et al.*, 2015a]. The first vertical dashed line (in green) marks the time of substorm dipolarization accompanied with sharp B_z enhancement (indicated by the first red arrow in Figure 1f, Dipolarization I) and was followed by rapid B_x decrease (Figure 1d) and intense field perturbations in all three components (Figures 1d – 1f). Around ~ 3 minutes later, MESSENGER detected another dipolarization (the second red arrow in Figure 1f, Dipolarization II)

when spacecraft was very near the center of the current sheet (B_x ~ 0 nT in Figure 1d, marked by the second vertical dashed line). The dipolarizations and intense field perturbations in July 1st event reveal the intense magnetospheric activities during this plasma sheet pass. In contrast in September 28th event, MESSENGER did not observe the features for dipolarization neither field perturbations, indicating this plasma sheet pass was during a quiet period in Mercury's magnetosphere. The September 28th event will be used as a reference for quiet magnetospheric conditions from now on. The July 1st and September 28th events shared similar plasma sheet crossing geometries.

We have performed Harris current sheet fitting for both events in the southern hemisphere (see next section for detail descriptions of Harris current sheet fitting). The fitting results are shown as the red dashed lines in Figures 1d and 1k. The current sheet half thickness for quiet period September 28th event is ~ 0.76 R_M, which is much thicker than the active period current sheet ~ 0.22 R_M of the July 1st event. Current sheet thickness differences between the Mercury's magnetospheric active and quiet periods suggested that the current sheet thickness during active period is smaller than the quiet period current sheet in a similar location.

Plasma sheet protons in the September 28th event were observed to mostly have energies lower than ~ 5 keV (Figure 1h). Protons in the July 1st event before the first dipolarization (Figure 1f, Dipolarization I) displayed a similar feature (Figure 1a). Such a 5 keV energy likely represent an upper limit for plasma sheet protons in quiet periods. We focus on supra-thermal protons, those with ≥ 4.68 keV (lower energy for FIPS energy channel including 5 keV), as compared to the plasma sheet protons that have typical thermal energies of ≤ 3 keV [*Gershman et al.*, 2014]. The supra-thermal

protons with energy > 3 keV is also evaluated in Section 2.2. The proton Supra-Thermal Particle Fluxes (STPF) were lower than ~ 3×10^6 $[cm^2s]^{-1}$ before Dipolarization I in the July 1st event and during the whole plasma sheet pass in the September 28th event (Figures 1b and 1i). A prominent increase in STPF from ~ 10^6 to 10^8 $[cm^2s]^{-1}$ (Figure 1b) was observed in the July 1st event after the Dipolarization I, which indicates that protons were effectively energized during this Mercury's dipolarization. The energization of protons could be due to the electric field induced by magnetic field dipolarization as shown in *Delcourt et al.* [2007]. The proton temperature (T_p, Figure 1c) were also increased from ~ 10 MK (1 MK = 10^6 K) to ~ 30 MK accompanying the dipolarization. The T_p increment reveals a heating process for protons during the substorm dipolarization. In the September 28th event, T_p (Figure 1j) were mostly lower than 10 MK. It needs to be noted that MESSENGER was located in the high-latitude plasma sheet during the Dipolarization I, so that proton energization and heating could be influenced by the afterward plasma sheet expansion [*Sun et al.*, 2015a] as the spacecraft moved towards the plasma sheet center. MESSENGER was very near the plasma sheet center during Dipolarization II (Figure 1f). The increments of STPF and T_p accompanying Dipolarization II shown in Figures 1b and 1c further support the proton energization and heating processes during Mercury's dipolarization.

In the Earth's plasma sheet, multi-components in ion distributions are frequently observed [e.g., *Christon et al.*, 1988; *Seki et al.*, 2003; *Wing et al.*, 2005]. The cold component suggested from the magnetosheath was present everywhere in the plasma sheet [*Wing et al.*, 2005]. The hot component, which is the nominal plasma sheet ions, can be fitted with a Kappa distribution [e.g., *Christon et al.*, 1988; *Wing et al.*, 2005]. The Kappa distribution function is given by [e.g., *Vasyliunas*, 1968; *Pierrard and*

Lazar, 2010],

$$f_i^{\kappa}(v) = \frac{n_i}{2\pi(\kappa\omega_{\kappa i}^2)^{3/2}} \frac{\Gamma(\kappa+1)}{\Gamma(\kappa-1/2)\Gamma(3/2)} \left(1 + \frac{v^2}{\kappa\omega_{\kappa i}^2}\right)^{-\kappa-1} \quad (1)$$

where v is the velocity of particles, $\omega_{\kappa i} = \sqrt{(2\kappa-3)k_B T_i/\kappa m_i}$ the thermal velocity, m_i the mass of particle, n_i the number density, T_i the equivalent temperature, $\Gamma(x)$ the Gamma function and k_B the Boltzmann constant. The index κ determines the slope of supra-thermal particle tail in the distribution. κ decrease indicates the decrease in the slope of supra-thermal particle tail, i.e., the increase in flux at higher energies, and therefore, the energization of particles. A Kappa distribution transforms into a Maxwellian as κ approach infinity ($\kappa \to \infty$). As a matter of fact, a Kappa distribution would be very near Maxwellian when $\kappa \geq 10$ [e.g., *Wing et al.*, 2005; *Pierrard and Lazar*, 2010].

To examine the energization and heating processes in more details during our two dipolarizations events, we fit them to two-component Kappa distributions. The averaged proton phase space density (PSD) from ~ 19:24:24 to ~ 19:24:43 UT (two scans) prior to the Dipolarization I is shown in Figure 2a. The corresponding counts in each energy channel are shown in Figure 2b. We have excluded data points with single counts (the red dots) during the fitting. This distribution contains two components. The component that contains higher T_p is called hot component, and the other cold component. The hot component is fit with a Kappa distribution (blue line), and cold component fit with a Gaussian (green line). Magnetosheath ions in Mercury's tail are frequently observed [e.g., *Sundberg et al.*, 2012], which could be one possible source for the cold component as indicated in Earth's study. The properties of cold components in Mercury's plasma sheet deserve a detail investigation in the future study.

Before Dipolarization I (Figure 2a), the hot component gives κ ~ 28.17 ± 3.04 and T_p ~ 7.8 ± 0.8 MK (in blue), and cold component gives T_p ~ 3.07 ± 2.38 MK (in green). After the Dipolarization I (Figure 2c) the distribution is well fit with a single Kappa distribution without a cold component, which gives κ ~ 2.65 ± 0.3 and T_p ~ 18.1 ± 2.0 MK. The increase in T_p and decrease in κ clearly reveal the heating and energization processes for protons during this dipolarization. The disappearance of the cold component after Dipolarization I (from Figure 2a to Figure 2c) may mean that the thermal protons were energized to supra-thermal during the dipolarization. It is also possible that the cold component was too tenuous to be detected by FIPS, i.e., below the one count level. As with all plasma instruments, FIPS sensitivity increased with increasing energy, so that the one count level for supra-thermal energies (defined previously as > 4.68 keV) was significantly lower than in the thermal range. The fits before and after the Dipolarization II, which was near the plasma sheet center, are displayed in Figures 2e and 2g. These fits give similar results as for Dipolarization I (Figures 2a and 2c): protons were energized (κ decrease from ~ 2.72 ± 0.39 to ~ 2.47 ± 0.29) and heated (T_p increase from ~ 24.9 ± 3.5 MK to ~ 46.2 ± 5.4 MK) during the dipolarization. In the fitting of Figure 2g, we have excluded the two data points below 1 keV with two counts. The two points might indicate the existence of another component, but there are not sufficient counts to determine this. The κ decrease during Dipolarization II is not as prominent as observed in Dipolarization I. This could because κ is already very small (~ 2.72 ± 0.39, pre-energized) before the Dipolarization II, while the energization of protons is clear since protons with energy lower than ~ 3 keV are hardly observed after Dipolarization II.

To further validate our results, we have also computed proton moments around the

two dipolarizations with the methods introduced in *Raines et al.* [2011] and *Gershman et al.* [2013]. We accumulated counts over the same four time intervals as described above and shown in Figure 2. We found that T_p from this method were ~ 7.3 MK and ~ 18.0 MK before and after Dipolarization I, respectively, and were ~ 19.0 MK and ~ 48.0 MK before and after the Dipolarization II. The result of heating by dipolarization is also evident in these temperatures, and does not depend on the use of the Kappa function.

The above case study reveals that dipolarization can effectively energize and heat the protons in the near Mercury tail. Therefore, a broader investigation of proton properties in the near Mercury tail, including STPF and T_p, would be very important in revealing the near Mercury tail dynamics. We performed a statistical study focusing on these parameters in the next section.

2.2. Statistical Results

The plasma sheet proton properties were distinct between the magnetospheric active (July 1st event after Dipolarization I) and quiet (September 28th event) periods**.** This is consistent with the results that fast upstream solar wind velocity corresponds to high proton temperature and slow solar wind corresponds to low temperature in Mercury's magnetotail [*Gershman et al.*, 2014]. As the magnetospheric disturbances are well correlated with solar wind speed, with fast solar wind corresponding to active period and slow solar wind the quiet period of the magnetosphere [e.g., *Sheeley et al.*, 1977]. Thus, it is necessary to separate the active periods plasma sheets from the quiet periods in the statistical study. The two events in Figure 1 have suggested that the current sheet thickness during active period would be smaller than the quiet period

current sheet in the similar location. Therefore, in this study, we apply the current sheet thickness to separate the Mercury's active periods' plasma sheet from that in the quiet periods. This study uses Harris current sheet model to derive the current sheet half thickness for each plasma sheet pass.

The magnetotail magnetic field profile is assumed to be comply with the one dimensional Harris current sheet model [*Harris*, 1962]:

$$B_{xy}(z) = B_L \tanh\left(\frac{z - z_0}{L}\right) \quad (2)$$

where B_{xy} is the measured magnetic field in local coordinates [e.g., *Poh et al.*, 2017a; *Rong et al.*, 2011], B_L the lobe field intensity, z_0 the position of the current sheet center (i.e., B_x reversal point determined in the 5 minutes moving mean magnetic field data), and L the current sheet half thickness. We also introduce χ^2 to judge the fitting results:

$$\chi^2 = \frac{1}{N}\sum_{i=1}^{N}\left(\left|B'_{xy}(i) - B_{xy}(i)\right| / \left|B'_{xy}(i)\right|\right)^2 \quad (3)$$

where N is the data point number, B_{xy}'(i) the model provided magnetic field, B_{xy}(i) the spacecraft measured field. We have averaged the magnetic field with a 40 s sliding window prior to the fitting, aiming to remove the field perturbations commonly observed in Mercury's plasma sheet. For example, flux ropes often last ~ 3 to 5 s [e.g., *Slavin et al*., 2012; *DiBraccio et al.*, 2015; *Sun et al.*, 2016]. Because of the high-latitude periapsis (> ~60°N) of MESSENGER orbits, the spacecraft is much closer to the planet and thus detects a stronger dipole magnetic field when it is in the northern hemisphere. We only fit the southern part of the plasma sheet measurements (i.e., $B_x < 0$) to get the current sheet half thickness, as in *Poh et al.* [2017a]. We consider the cases with $\chi^2 < 0.05$ to be good fits.

Because this study focuses on the near Mercury tail region, we fit the plasma sheet in the region with X'_{MSM} between -1.0 R_M and -1.8 R_M, Y'_{MSM} between 1.8 R_M and -1.8 R_M. There are 1225 cases satisfying the above criteria. We then output the STPF and T_p for each plasma sheet crossing, considering the mean values in four minutes around plasma sheet center (i.e., the B_x reversal points). Figures 3a and 3d display the distributions of STPF and T_p in all the 1225 cases and clearly show that STPF and T_p are higher in the near Mercury region (R < ~ 1.5 R_M, $R = \sqrt{X_{MSM}^2 + Y_{MSM}^2}$). The dawn-dusk asymmetry features can be found in both figures with STPF and T_p higher on the dawnside plasma sheet than the duskside.

To further examine the features in these distributions, we divided the cases in each bin into two categories, the thin current sheets (thin CSs, corresponding to Mercury's magnetospheric active periods), and the thick current sheets (thick CSs, corresponding to quiet periods). We define the current sheets with thicknesses smaller than the mean thickness in each bin as thin CSs, and the others thick CSs. The STPF distributions of thin CSs and thick CSs are shown in Figures 3b and 3c, and T_p in Figures 3e and 3f, respectively. During the magnetospheric active periods in thin CSs, STPF (Figure 3b) is predominantly higher on the dawnside than the duskside in the near Mercury region, and T_p (Figure 3e) shows a similar feature. But, STPF and T_p during the magnetospheric quiet periods in thick CSs (shown in Figures 3c and 3f) do not exhibit clearly dawn-dusk asymmetry features. The local time distributions for STPF are shown in Figure 3g. There are no large differences for STPF between Thin CSs and Thick CSs in the pre-midnight regions (21:00 to 00:00, ~ 1.5×10^7 $cm^{-2}s^{-1}$). However, the STPF for Thin CSs (> 2×10^7 $cm^{-2}s^{-1}$) is larger than for Thick CSs (~ 1.5×10^7 $cm^{-2}s^{-1}$) in local time bins from 00:00 to 02:00. The T_p distributions in Figure 3h show similar features as STPF. T_p in the pre-midnight regions do not display large

differences between Thin CSs and Thick CSs, but in Thin CSs are at least 10 MK larger Thick CSs in the post-midnight regions. Therefore, we conclude that proton energization and heating processes are more intense in the dawnside of near Mercury tail during magnetospheric active periods. It needs to be noted that fluxes for protons with energy higher than ~ 3.2 keV show similar distributions as particle flux higher than ~ 4.68 keV employed in this study. And the cases with χ^2 < 0.03 (1033 cases) also revealed similar results as χ^2 < 0.05 displayed in Figure 3.

Considering the prominent dawn-dusk asymmetry of STPF and T_p during the active periods, it would be meaningful to check the features of B_z variations, i.e., the dipolarization, in the near Mercury tail region. We have selected out the largest B_z increase in 5 s (δB_{zmax}) after subtracting a 40 s moving mean background magnetic field for the 1225 plasma sheet passes used in Figure 3. We apply a 40 s sliding window to obtain background magnetic field aiming to average over the small magnetic structures, the same as we have done during Harris current sheet fitting. The time scale of 5 s for the selection of δB_{zmax} is due to substorm dipolarization only last ~ 5 s at Mercury [e.g., *Sun et al.*, 2015a]. Figures 4a to 4c show these δB_{zmax} distributions. A clear dawn-dusk asymmetry feature is present, with δB_{zmax} larger on the dawnside than the duskside for all CSs (Figure 4a). This feature is more prominent for the distribution in thin CSs (Figure 4b), but is not clear in thick CSs (Figure 4c). This δB_{zmax} feature explicitly indicates that dipolarizations were more frequently observed in the dawnside plasma sheet at Mercury. Computing δB_{zmax} in a 10 s window or subtracting a 60 s moving mean background magnetic field do not change the dawn-dusk asymmetry feature. In order to investigate the heliocentric distance effects for the dawn dusk asymmetry, we have shown the heliocentric distance distributions for all the tail current sheet crossings (Figures 4d to 4e) in different years.

Figure 4d is for the tail current sheet crossings in 2011 and 2012, and Figure 4e for the years from 2013 to 2015. It shows that the heliocentric distance distributions in the two figures are almost opposite to each other. There is no local time dependence for the heliocentric distances for the tail current sheets investigated in this study. Therefore, the heliocentric distance would not be able to create effective local time dependence in proton temperature, STPF, and δB_{zmax}.

3. Conclusion and Discussion

MESSENGER observations have revealed the enhancements of STPF (i.e., energization) and temperatures (i.e., heating) for protons during Mercury's dipolarizations using FIPS measurements. Case analysis has shown that Mercury's plasma sheet protons contain two components, cold and hot, with the hot component being well fit with Kappa distribution. In the distribution before the Dipolarization I (Figure 2a), κ was ~ 28 for the hot component, indicating that this distribution was very close to Maxwellian [e.g., *Wing et al.*, 2005; *Pierrard and Lazar*, 2010]. But in the distribution after Dipolarization I, κ was smaller than 3 for this component. The sharp κ decrease implies strong proton energization during dipolarization at Mercury, which might also an indication for the existence of strong wave-particle interactions during the dipolarization [e.g., *Miller*, 1991; *Schizgal*, 2007]. At the same time, we also observed T_p increases indicating heating of plasma sheet protons during Mercury's substorm dipolarization.

The STPF and T_p distributions in the near Mercury tail show clear dawn-dusk asymmetry features with STPF and T_p much higher on the dawnside than the duskside. This feature is more prominent during the Mercury's magnetospheric active periods, but is not clear in the quiet times. Our study of δB_{zmax} variations in Mercury's plasma

sheet shows similar dawn-dusk asymmetry features. The proton and δB_{zmax} distributions, in conjunction with the case results, indicate that substorm dipolarization at Mercury would be more frequently initiated in the dawnside plasma sheet, i.e., the postmidnight sector, than the duskside. Dawnside initiated substorm dipolarizations would energize and heat protons more prominently in the dawnside plasma sheet, resulting in STPF and T_p values which are much higher on the dawnside. In previous observations, energetic electron events were prominently observed on the dawnside magnetosphere of Mercury [e.g., *Baker et al.*, 2016; *Ho et al.*, 2016; *Lindsay et al.*, 2016]. This dawn-dusk asymmetry could be due to the energizations electrons by dipolarizations locally on the dawnside of Mercury's magnetosphere, in addition to dawnward gradient-curvature drift. The dawnside locations of substorm dipolarizations would also imply that flow braking more frequently occurs on the dawnside at Mercury.

This study shows that the proton properties and dipolarizations in the near Mercury tail display the features similar to reconnection locations in the NMNL [*Sun et al.*, 2016]. STPF and T_p are much higher on the dawnside tail than the duskside, and dipolarizations are more frequently observed on the dawnside than the duskside. These features are opposite from those observed at Earth, where magnetic reconnection occurred more often in the duskside plasma sheet [e.g., *Nagai et al.*, 2013] and ion and electron dispersionless injections were more frequently observed in the pre-midnight plasma sheet [e.g., *Gabrielse et al.*, 2014].

Acknowledgement.

The data used in this study were available from the Planetary Data System (PDS): http://pds.jpl.nasa.gov. The MESSENGER project is supported by the NASA Discovery Program under contracts NASW-00002 to the Carnegie Institution of Washington and NAS5-97271 to The Johns Hopkins University Applied Physics Laboratory. WJS is funded by National Postdoctoral Program for Innovative Talents (grant BX201600158) and China Postdoctoral Science Foundation (grant 2016M600124). This work is supported by the National Nature Science Foundation of China (grants 41525016, 41474155, 41474139, 41661164034). YW is supported by Thousand Young Talents Program of China. The contributions by one of the authors (JAS) were supported by NASA's Heliophysics Supporting Research (NNX15AJ68G) and Living With a Star (NNX16AJ67G) programs. ZY is a Marie-Curie COFUND postdoctoral fellow at the University of Liege. Co-funded by the European Union. This work is also supported by the CAS Key Laboratory of Lunar and Deep Space Exploration through grant 2013DP173157. Wei-Jie Sun thanks Dr. Haje Korth (The Johns Hopkins University Applied Physics Laboratory), Dr. Yongfu Wang (School of Earth and Space Sciences, Peking University) and Dr. Jun Zhong (Key Laboratory of Earth and Planetary Physics, Chinese Academy of Sciences) for helpful discussions.

References

Anderson, B. J., et al. (2007), The Magnetometer Instrument on MESSENGER, *Space Sci Rev*, 131(1-4), 417-450.

Andrews, G. B., et al. (2007), The Energetic Particle and Plasma Spectrometer Instrument on the MESSENGER Spacecraft, *Space Sci Rev*, 131(1-4), 523-556.

Baker, D. N., et al. (2016), Intense energetic electron flux enhancements in Mercury's magnetosphere: An integrated view with high-resolution observations from MESSENGER, *J. Geophys. Res.*, 121(3), 2171-2184.

Christon, S. P., et al. (1979), Electron calibration of instrumentation for low energy, high intensity particle measurements at Mercury, *J. Geophys. Res.*, 84(A8), 4277-4288.

Christon, S. P. (1987), A comparison of the Mercury and Earth magnetospheres: Electron measurements and substorm time scales, *Icarus*, 71(3), 448-471.

Christon, S. P., et al. (1988), Energy spectra of plasma sheet ions and electrons from ~50 eV/e to ~1 MeV during plasma temperature transitions, *J. Geophys. Res.*, 93(A4), 2562-2572.

Delcourt, D. C., et al. (2007), Ion energization during substorms at Mercury, *Planet Space Sci*, 55(11), 1502-1508.

DiBraccio, G. A., et al. (2015), MESSENGER observations of flux ropes in Mercury's magnetotail, *Planet Space Sci*, 115, 77-89.

Gabrielse, C., et al. (2014), Statistical characteristics of particle injections throughout the equatorial magnetotail, *J. Geophys. Res.*, 119(4), 2512-2535.

Gershman, D. J., et al. (2013), Magnetic flux pileup and plasma depletion in Mercury's subsolar magnetosheath, *J. Geophys. Res.*, 118(11), 7181-7199.

Gershman, D. J., et al. (2014), Ion kinetic properties in Mercury's premidnight plasma sheet, *Geophys. Res. Lett.*, 41, 5740–5747, doi:10.1002/2014GL060468.

Harris, E. G. (1962), On a plasma sheath separating regions of oppositely directed magnetic field, *Nuovo Cimento*, 23, 115–121.

Ho, G. C., et al. (2016), MESSENGER observations of suprathermal electrons in Mercury's magnetosphere, *Geophys. Res. Lett.*, 43(2), 550-555.

Ip, W. (1997), Time-variable phenomena in the magnetosphere and exosphere of Mercury, *Adv Space Res*, 19(10), 1615-1620.

Korth, H., et al. (2014), Plasma distribution in Mercury's magnetosphere derived from MESSENGER Magnetometer and Fast Imaging Plasma Spectrometer observations, *J. Geophys. Res.*, 119(4), 2917-2932.

Lindsay, S. T., et al. (2016), MESSENGER X-ray observations of magnetosphere–surface interaction on the nightside of Mercury, *Planet Space Sci*, 125, 72-79.

Lopez, R. E., et al. (1990), The energetic ion substorm injection boundary, *J. Geophys. Res.*, 95(A1), 109-117.

Miller, J. A. (1991), Magnetohydrodynamic turbulence dissipation and stochastic proton acceleration in solar flares, *The Astrophysical Journal*, 376, 342-354.

Nagai, T., et al. (1998), Structure and dynamics of magnetic reconnection for substorm onsets with Geotail observations, *J. Geophys. Res.*, 103(A3), 4419-4440.
Nagai, T., et al. (2013), Three-dimensional structure of magnetic reconnection in the magnetotail from Geotail observations, *J. Geophys. Res.*, 118(4), 1667-1678.
Pierrard, V., and M. Lazar (2010), Kappa Distributions: Theory and Applications in Space Plasmas, *Sol Phys*, 267(1), 153-174.
Poh, G., et al. (2017a), Mercury's cross-tail current sheet: Structure, X-line location and stress balance, *Geophys. Res. Lett.*, 44(2), 678-686.
Raines, J. M., et al. (2011), MESSENGER observations of the plasma environment near Mercury, *Planet Space Sci*, 59(15), 2004-2015.
Raines, J. M., et al. (2014), Structure and dynamics of Mercury's magnetospheric cusp: MESSENGER measurements of protons and planetary ions, *J. Geophys. Res.*, 119(8), 6587-6602.
Rong, Z. J., et al. (2011), Statistical survey on the magnetic structure in magnetotail current sheets, *J. Geophys. Res.*, 116(A9), n/a-n/a.
Shizgal, B. D. (2007), Suprathermal particle distributions in space physics: Kappa distributions and entropy, *Astrophys Space Sci*, 312(3), 227-237.
Seki, K., et al. (2003), Cold ions in the hot plasma sheet of Earth's magnetotail, *Nature*, 422(6932), 589-592.
Sheeley, N.R., et al. (1977) A pictorial comparison of interplanetary magnetic field polarity, solar wind speed, and geomagnetic disturbance index during the sunspot cycle, *Sol. Phys.*, 52: 485-495. doi:10.1007/BF00149663
Slavin, J. A., et al. (1997), Mariner 10 observations of field-aligned currents at Mercury, *Planet Space Sci*, 45(1), 133-141.
Slavin, J. A., et al. (2010). MESSENGER observations of extreme loading and unloading of Mercury's magnetic tail. *Science*, 329, 665–668. doi:10.1126/science.1188067.
Slavin, J. A., et al. (2012), MESSENGER and Mariner 10 flyby observations of magnetotail structure and dynamics at Mercury, *J. Geophys. Res.*, 117, A01215, doi:10.1029/2011JA016900.
Slavin, J. A., et al. (2014), MESSENGER observations of Mercury's dayside magnetosphere under extreme solar wind conditions, *J. Geophys. Res.*, 119(10), 8087-8116.
Solomon, S., R. L. McNutt Jr., R. E. Gold, and D. L. Domingue (2007), MESSENGER mission overview, *Space Sci. Rev.*, 131(1-4), 3–39, doi:10.1007/s11214-007-9247-6.
Sun, W.-J., et al. (2015a), MESSENGER observations of magnetospheric substorm activity in Mercury's near magnetotail. *Geophys. Res. Lett.*, 42, 3692–3699. doi: 10.1002/2015GL064052.
Sun, W.-J., et al. (2015b), MESSENGER observations of Alfvénic and compressional waves during Mercury's substorms. *Geophys. Res. Lett.*, 42, 6189–6198. doi: 10.1002/ 2015GL065452.

Sun, W. J., et al. (2016), Spatial distribution of Mercury's flux ropes and reconnection fronts: MESSENGER observations, *J. Geophys. Res.*, 121(8), 7590-7607.
Sundberg, T., et al. (2012), MESSENGER orbital observations of large-amplitude Kelvin-Helmholtz waves at Mercury's magnetopause, *J. Geophys. Res.*, 117(A4).
Sundberg, T., et al. (2012), MESSENGER observations of dipolarization events in Mercury's magnetotail, *J. Geophys. Res.*, 117(A12), A3M.
Sundberg, T. and Slavin, J. A. (2015) Mercury's Magnetotail, in *Magnetotails in the Solar System* (eds A. Keiling, C. M. Jackman and P. A. Delamere), John Wiley & Sons, Inc, Hoboken, NJ. doi: 10.1002/9781118842324.ch2
Vasyliunas, V. M. (1968), A survey of low-energy electrons in the evening sector of the magnetosphere with OGO 1 and OGO 3, *J. Geophys. Res.*, 73(9), 2839-2884.
Wing, S., et al. (2005), Dawn-dusk asymmetries, ion spectra, and sources in the northward interplanetary magnetic field plasma sheet, *J. Geophys. Res.*, 110(A8).
Zurbuchen, T. H., et al. (2011), MESSENGER observations of the spatial distribution of planetary ions near Mercury, Science, 333, 1862–1865, doi:10.1126/science.1211302.

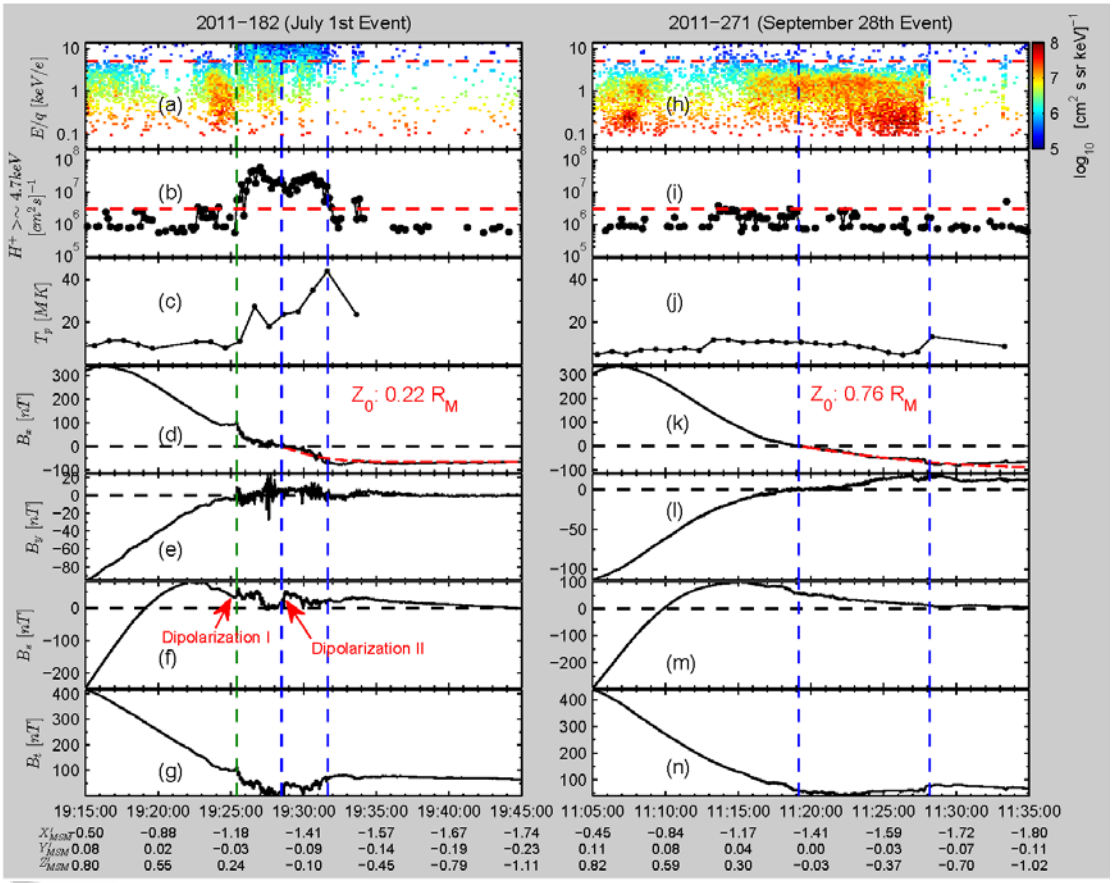

Figure 1. Overview of proton and magnetic field measurements from MESSENGER plasma sheet crossings on July 1, 2011 (left column) and September 28, 2011 (right column). (a, h) Proton energy spectra in the unit of differential particle flux, (b, i) particle flux for protons with energy from ~ 4.68 keV to ~ 13.6 keV (STPF), (c, j) proton temperature T_p, (d, k) B_x, red dashed lines are from the fit Harris current sheet models, Z_0 are the current sheet half thickness obtained from model, (e, l) B_y, (f, m) B_z, (g, n) B_t. The two blue vertical dashed lines indicate the center and south edge of plasma sheet. The green vertical dashed line in July 1st event marks the time of substorm dipolarization as identified by *Sun et al.* [2015a]. The two red arrows in Figure 1f indicate the Dipolarization I and Dipolarization II, respectively.

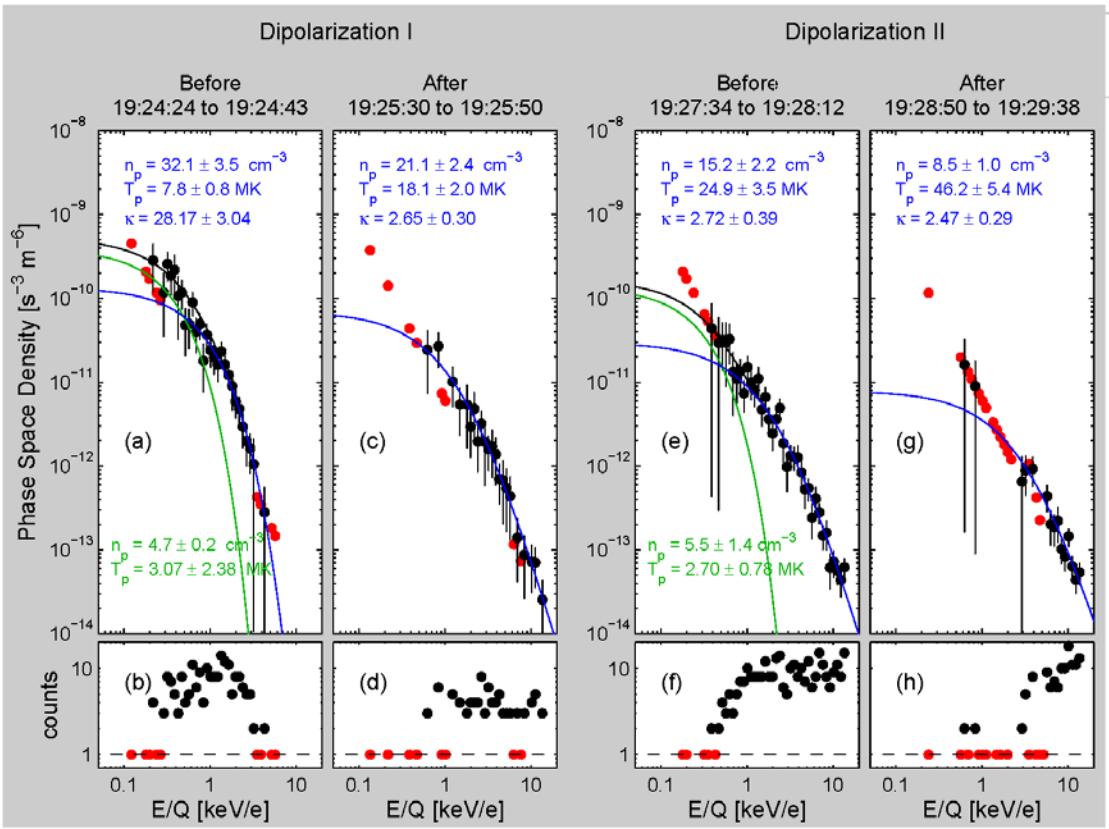

Figure 2. Proton phase space (PSD) densities and counts versus E/Q before and after the two dipolarizations in 1 July 2011 crossing. (a, b) and (c, d) show PSD and counts before and after Dipolarization I, respectively. (e, f) and (g, h) are for Dipolarization II. Red dots in each figure represent the data points with one counts. Blue lines in (a, c, e, g) are the Kappa fitting results for hots components. Green lines in (a, e) are the Maxwellian fitting for cold components. Black lines in (a, e) are the sum of blue and green lines.

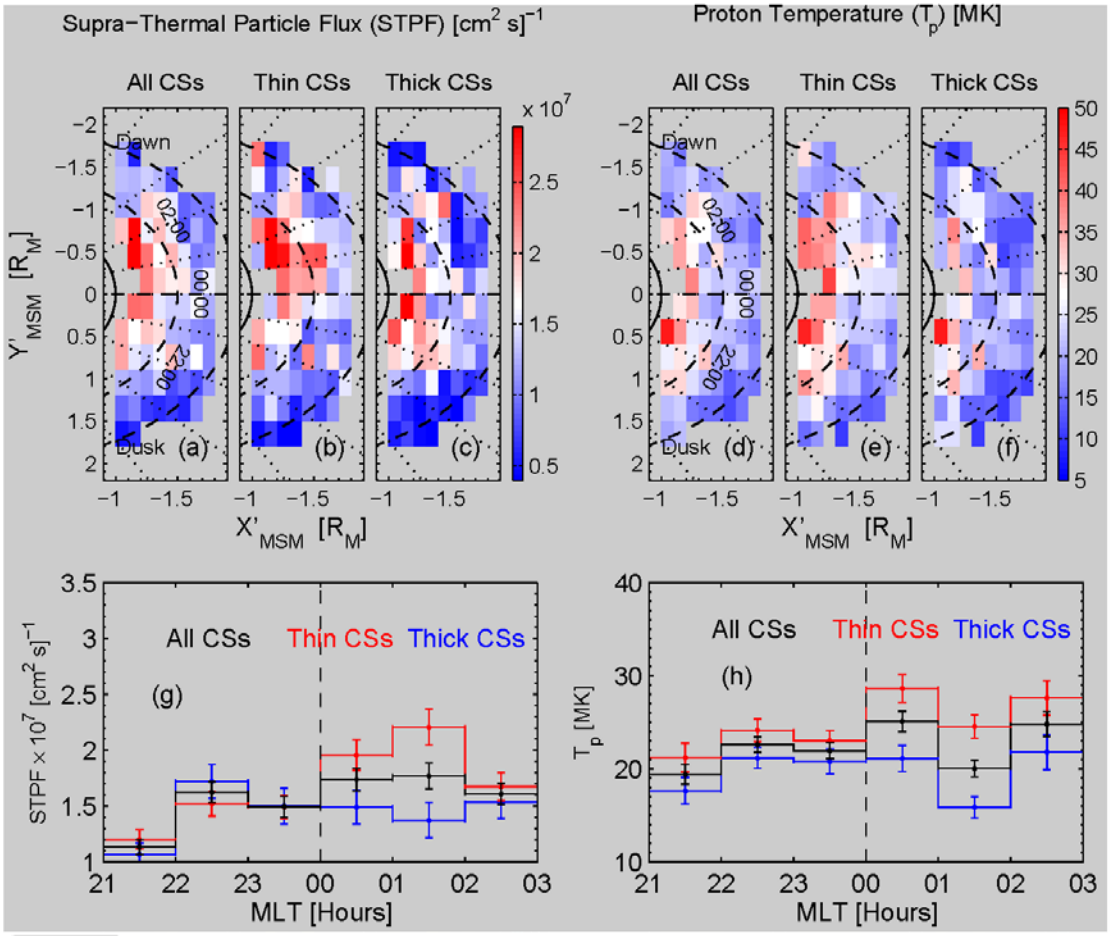

Figure 3. Equatorial distributions of STPF (a, b, c) and T_p (d, e, f) in the near Mercury tail region. All CSs (a, d) are all plasma sheet passes with good Harris current sheet model fits ($\chi^2 < 0.05$). Thin CSs (b, e, corresponding to quiet periods) are thin current sheets in each bin, and Thick CSs (c, f, corresponding to active periods) are thick current sheets in each bin. We define the current sheets with thicknesses smaller than the mean thickness in each bin as thin CSs, and the others thick CSs. The number of events in each bin is > 5 in (a, d), and is > 2 in (b, c, e, f). The distributions of STPF (g) and T_p (h) with magnetic local times. Black lines are for All CSs, red lines for Thin CSs, and blue lines for Thick CSs, respectively. The error bars are the standard deviations in each local time bin.

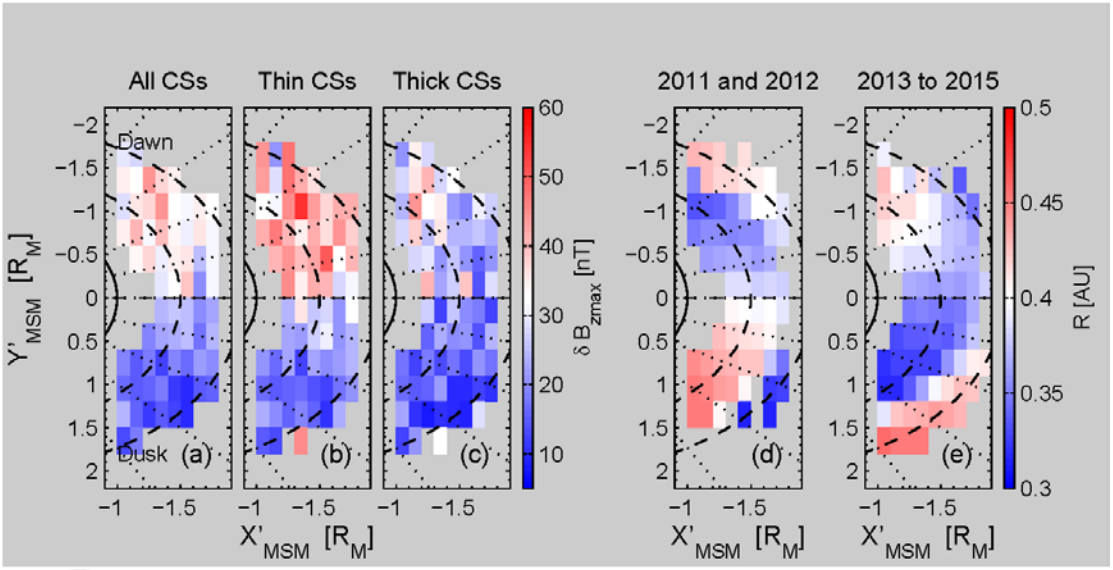

Figure 4. Equatorial distributions for δB_{zmax} and heliocentric distances (R). Panels (a, b, c) are in the same format as (a, b, c) or (d, e, f) in Figure 3. The distribution of mean heliocentric distances for the tail current sheet crossings in 2011 and 2012 (d), and from 2013 to 2015 (e).